Optofluidic distributed feedback lasers with evanescent pumping: Reduced threshold and angular dispersion analysis

Markus Karl, Guy L. Whitworth, Marcel Schubert, Christof P. Dietrich, Ifor D. W. Samuel, Graham A. Turnbull, and Malte C. Gather

Citation: Applied Physics Letters **108**, 261101 (2016); doi: 10.1063/1.4954650
View online: http://dx.doi.org/10.1063/1.4954650
View Table of Contents: http://scitation.aip.org/content/aip/journal/apl/108/26?ver=pdfcov
Published by the AIP Publishing

Optofluidic distributed feedback lasers with evanescent pumping: Reduced threshold and angular dispersion analysis

Markus Karl, Guy L. Whitworth, Marcel Schubert, Christof P. Dietrich, Ifor D. W. Samuel, Graham A. Turnbull, and Malte C. Gather[a)]
Organic Semiconductor Centre, SUPA, School of Physics and Astronomy, University of St Andrews, St Andrews, Fife KY16 9SS, United Kingdom

(Received 24 March 2016; accepted 2 June 2016; published online 27 June 2016)

We demonstrate an evanescently pumped water-based optofluidic distributed feedback (DFB) laser with a record low pump threshold of $E_{TH} = 520\,\text{nJ}$. The low threshold results from an optimized mode shape, which is achieved by a low refractive index substrate, and from the use of a mixed-order DFB grating. Investigating the photonic band structure via angular dispersion analysis both above and below lasing threshold allows us to measure the refractive index of the liquid gain layer and to determine the device parameters such as the waveguide core layer thickness. We show that it is possible to tailor the divergence of the lasing emission by varying the number of second order grating periods used for outcoupling. [http://dx.doi.org/10.1063/1.4954650]

Distributed feedback (DFB) lasers are one of the most versatile and efficient laser structures. Examples include DFB semiconductor lasers for telecommunications,[1] polymer based organic lasers for explosive sensing,[2] nanoimprinted vitamin,[3] and DNA[4] lasers for bio applications and single mode optofluidic DFB lasers.[5–7] Especially, optofluidic DFB lasers have attracted substantial attention due to their potential for cost-effective lab-on-a-chip spectroscopy applications.[8,9] Compared with whispering gallery mode resonators and Fabry–Pérot like cavities, the DFB structure is particularly well suited for achieving narrow bandwidth single-mode lasing operation. Single-mode operation is often desirable, e.g., for high resolution spectroscopy and sensing, in part because it simplifies the monitoring of changes in the emission spectrum. Moreover, the periodic structure of DFB gratings gives rise to a well-defined photonic band structure which allows the measurement of optical parameters even below threshold.[10,11]

The most common design for optofluidic DFB lasers is based on a gain doped liquid core waveguide structure as this configuration readily satisfies the need for a substantial overlap of the optical mode with the gain region.[12] However, such devices require the use of buffers or solvents with high refractive index, such as ethylene glycol or dimethyl sulfoxide (DMSO).[5–7,13,14] High refractive index solvents are usually not biocompatible, which limits the application of optofluidic DFB lasers in biosensing.[15]

The study of stimulated emission from biological materials has also gained substantial interest over the last two decades, from random lasing in dye stained animal tissue[16] to the development of single cell biological lasers.[17] However, in order to realize optofluidic DFB lasers with biocompatible water based gain fluids, an evanescent pumping scheme is required due to the relatively low refractive index of water. In this configuration, which was first proposed by Ippen and Shank in 1972,[18] a polymer based waveguide core is adjacent to the gain doped fluid layer. Although the stimulated emission rate is limited due to the reduced overlap of the laser-active optical mode with the gain layer, evanescent pumped DFB lasers have been demonstrated by Song *et al.* in 2009.[19] Despite this initial success, lasing thresholds have so far remained large compared with fluid-core DFB lasers, and DMSO had to be added to the dye solution in order to enhance the mode overlap, which has prevented more widespread application of this configuration.

In this work, we fabricated and investigated an aqueous-solution-based evanescently pumped optofluidic DFB laser. As illustrated in Fig. 1, the laser comprises a substrate as bottom cladding, a polymer film, into which a grating structure is imprinted, as waveguide core, and a water-based fluorescent dye solution as upper cladding layer. By utilizing a mixed order grating and a low index substrate, we were able to demonstrate low lasing threshold of $E_{TH} = 520\,\text{nJ}$ which represents nearly a 20-fold reduction over the previously reported values (earlier thresholds were $E_{TH} = 9.5\,\mu\text{J}$; Ref. 19). The photonic angular dispersion was measured using single shot Fourier imaging to relate the spectral and spatial

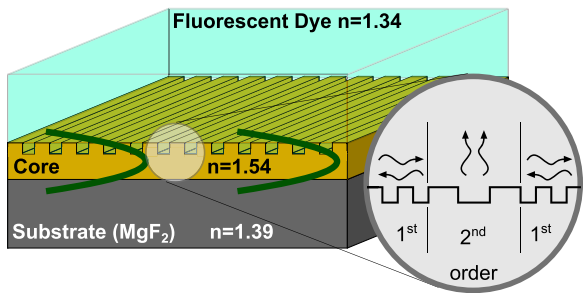

FIG. 1. Illustration of an optofluidic DFB laser. The waveguide stack consists of a substrate, a core-grating, and a gain material layer. The core layer has a thickness of several 100 nm and the substrate and gain layer have a thickness of ~1 mm. The refractive index of the core-grating layer is greater than the refractive indices of the adjacent layers. On the mixed-order grating, the 1st order is used for in plane feedback and the 2nd order for outcoupling perpendicular to the surface.

a)Email: mcg6@st-andrews.ac.uk

emission properties below and above lasing threshold to photonic modes. This enables measurements of the waveguide properties, such as the refractive index of the gain fluid, even below the lasing threshold.

To model our DFB laser structure, it was decomposed into an asymmetric waveguide and a grating structure. We chose a two-dimensional simulation approach because our structure is planar. For the DFB laser to operate efficiently, the waveguide needs to support and confine the optical modes. For a dielectric three layer slab waveguide, the optical modes fulfill the relation[20]

$$\frac{4\pi d}{\lambda_0}\sqrt{n_g^2 - n_{eff}^2} = \phi_a + \phi_s + 2M\pi\,, \tag{1}$$

where d is the thickness of the waveguide core, λ_0 is the vacuum wavelength, n_g the refractive index of the waveguide layer, n_{eff} the effective refractive index of the mode, $\phi_{a/s}$ the Goos–Hänchen phase shift at the interface between waveguide layer and each cladding layer, and M is an integer.

Light is Bragg scattered by the corrugation at the interface between the solid waveguide core and the liquid gain cladding layer. The scattering angle depends on the wavelength of the propagating mode and can be described by[21]

$$\frac{2\pi}{\lambda}\sin\theta = \pm\frac{2\pi n_{eff}}{\lambda} \pm m\frac{2\pi}{\Lambda}\,, \tag{2}$$

where λ is the wavelength, θ is the free-space scattering angle, Λ is the grating period, and m is an integer. Distributed feedback occurs when the grating diffracts the mode into the counter propagating mode, i.e., if the Bragg condition $m\lambda = 2n_{eff}\Lambda$ is satisfied.

Using Eq. (1) and solving the Helmholtz equation with appropriate boundary conditions, we determined the electric field distribution within the three layer dielectric waveguide. Fig. 2(a) shows the case for the TE0 mode. For an SiO_2 substrate (dashed line, $n_{SiO_2} = 1.46$) the mode is highly asymmetric, with a significant fraction of the mode located in the substrate. Therefore, the overlap factor Γ of the mode with the gain medium is only 11.7 % (assuming a core layer thickness of $d = 300$ nm). Changing the substrate material to MgF_2 ($n_{MgF_2} = 1.39$) renders the TE0 mode more symmetric, leading to an increased overlap with the gain layer ($\Gamma = 18.4$ %). This is due to the lower refractive index of MgF_2 compared with SiO_2.

The waveguide core thickness also influences the confinement of the mode and hence the overlap with the gain layer (Fig. 2(b)). For the MgF_2 substrate the mode overlap continues to increase with decreasing core thickness across the entire range modeled here. However, for the SiO_2 substrate it saturates for core layer thicknesses <300 nm with a cut-off thickness of $d_{cut} = 168$ nm. For all core layer thicknesses, the overlap for MgF_2 substrate exceeds the overlap for SiO_2-based devices. On an MgF_2 substrate, waveguide modes are no longer supported if the core layer thickness is reduced below 66 nm (not shown in Fig. 2(b)). For a layer thickness above 450 nm (MgF_2 substrate) and 700 nm (SiO_2 substrate), respectively, TE1 and TM1 modes are supported by the waveguide structure. Exceeding these thicknesses is not desirable as it could lead to mode beating and multi-mode lasing.

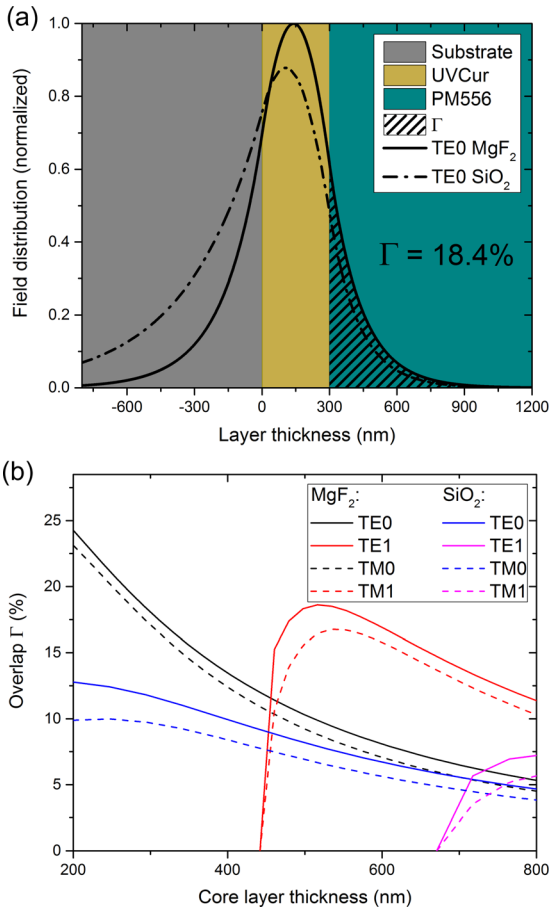

FIG. 2. (a) TE0 mode simulation for the waveguide stack formed by substrate, core-grating (UV-Cur06) and gain material (PM556). The dashed line shows the TE0 mode for a SiO_2 substrate for a core layer thickness of $d = 300$ nm. The overlap with the gain layer for this case is $\Gamma = 11.7\%$. The solid line shows the TE0 mode for an MgF_2 substrate. The mode is more symmetrical and an enhanced overlap with the gain layer of $\Gamma = 18.4\%$ is seen. (b) Simulated mode overlap with the gain layer for different core layer thicknesses, substrate materials, and polarizations (TE and TM). The highest overlap is achieved with MgF_2 substrates and a core layer thickness of $d < 300$ nm.

The DFB lasers fabricated here consist of a 25 mm × 25 mm MgF_2 or SiO_2 substrate, a UV-curable crosslinked polymer film as waveguide core (mr-UVCur06, Microresist Technologies , $n = 1.54$), and a dye doped water droplet as gain layer ($n = 1.34$). All stated refractive indices are for a wavelength $\lambda = 530$ nm. The mr-UVCur06 layer was spin coated onto the substrate, and by varying the spinning parameters, different layer thicknesses ranging from 250 nm to 600 nm were achieved. We used a UV-nanoimprint lithography process as described in detail by Wang *et al.*[22] to pattern the grating onto the mr-UVCur06 layer. A detailed characterization of this grating and corresponding SEM images can be found in Ref. 22.

To achieve low threshold lasing, a one dimensional mixed-order grating was used. Utilizing such a mixed-order grating, very low lasing thresholds down to 57 W/cm^2 were previously achieved for organic semiconductor based DFB lasers.[22] The grating used here consisted of two first-order regions, with 2860 grating periods of $\Lambda = 175$ nm, separated by a central second-order region, which had a grating period of $\Lambda = 350$ nm and between 4 and 12 repetitions. The total area of each grating was 1 mm × 1 mm. Due to Bragg

scattering, the first-order region supports in-plane optical feedback and the smaller second-order region provides surface outcoupling by scattering the mode out of plane perpendicular to the surface via first-order diffraction (see inset in Fig. 1).[2]

The gain layer consisted of an aqueous solution of the fluorescent dye Pyrromethene 556 (PM556, Disodium-1,3,5,7,8-pentamethylpyrromethene-2,6-disulfonate-difluoroborate, Exciton, Inc.). Concentrations of 0.8 to 5 mmol/l of PM556 were dissolved in deionized water and a droplet of the solution (10 μl) was then placed on the grating structure. The amount of dye solution was sufficient to avoid evaporation for more than 10 min of continuous pumping. In addition, photobleaching was avoided due to convection inside the droplet, which replenished the fluorophores in the volume close to the feedback structure.

In order to investigate the photonic band structure of our DFB structures, the DFB gratings were illuminated with a broad band halogen lamp through a microscope objective. The reflectance of the grating was collected with the same objective and the Fourier plane of the objective was imaged onto the entrance slit of a spectrometer in order to resolve the angle dependence of the reflectivity.[23] The structure transmits most of the incident light, but a fraction of the light is coupled to the waveguide and scattered back at the angles at which Eq. (2) is satisfied. In this way we were able to measure the angle dependent photonic dispersion over a range of $\pm 33^\circ$ using a $40\times$ ($NA = 0.55$) objective. A measurement of the photonic band structure of a SiO_2-based second-order DFB grating region with $\Lambda = 350$ nm and with air as the top layer is shown in Fig. 3(a). Fitting Eq. (2) to the photonic bands and solving Eq. (1) yields a core layer thickness of $d = (554 \pm 7)$nm, which is still below the onset thickness for TE1 and TM1 modes in SiO_2-based devices (Fig. 2(b)). As can be seen in the inset of Fig. 3(a), a characteristic photonic stop band opens at 0° angle and the resonance wavelength $\lambda_{res} = (527.7 \pm 0.2)$nm.

Next, the fluorescent dye solution was excited by direct pumping through the substrate and the grating (similar pump configuration as used by Song *et al.*[19]) using a pulsed optical parametric oscillator (OPO) system tuned to 480 nm (20 Hz repetition rate and 5 ns pulse length, pump energy <100 nJ). In this configuration, dye molecules in a volume above the waveguide are excited. Fig. 3(b) shows the angle-resolved photoluminescence of the grating discussed before, but now with a droplet of aqueous PM556 solution as the top layer. The data indicate that a portion of the fluorescence generated by the dye is coupled to the waveguide and then scattered to the top and bottom by the DFB grating. This led to a reduction in the recorded fluorescence signal along the photonic bands. Fitting Eq. (2) to the photonic bands and solving Eq. (1) yields a refractive index of the dye solution of $n = 1.342 \pm 0.015$.

In order to test lasing in the MgF_2-based structures, we increased the pump energy from the OPO. Using the same pump scheme, the image plane of the objective was now imaged onto the entrance slit of the spectrometer. The pump spot was aligned on the grating, for maximum emission intensity. Emission spectra for a range of pump energies are shown in Fig. 4(a). Below $E = 338$ nJ we observe a broad

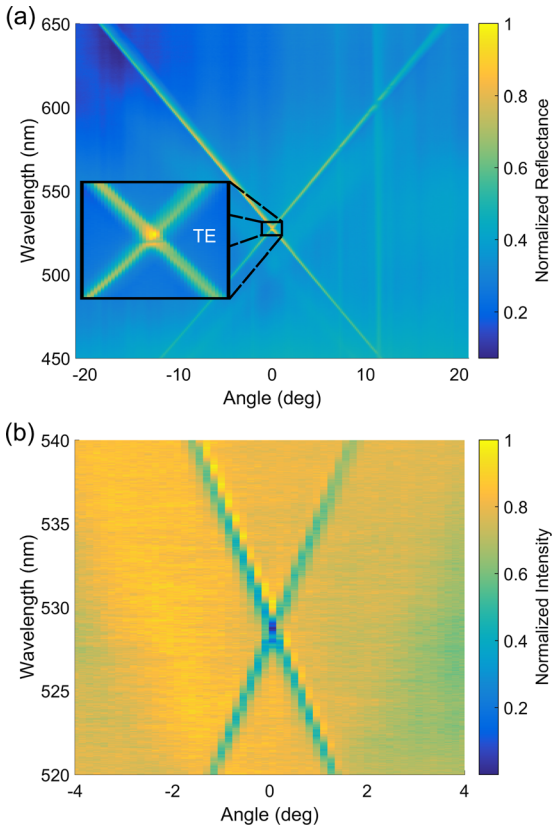

FIG. 3. Angular dispersion measurement. (a) Reflectance measurement of a SiO_2-based second-order DFB grating region with air as the top layer. Most of the light is transmitted and only a fraction is coupled to the waveguide and Bragg scattered back. The angular dispersion allows determining the core layer thickness. (Inset: Zoom-in of the region around the resonance wavelength). (b) Fluorescence measurement of the DFB grating with a dye droplet on top. A portion of the emitted fluorescence is coupled to the waveguide and scattered in both directions by the DFB grating. This leads to a reduced signal along the photonic band structure. The pump power during the measurement shown here was well below the lasing threshold.

emission spectrum, attributed to background fluorescence from the dye. At $E = 667$ nJ, a weak peak starts to appear and then quickly gains in absolute and relative intensity as the pump pulse energy is increased further. The width of this peak is below the resolution limit of the spectrometer ($\Delta\lambda < 0.07$ nm). We attribute the peak to single mode laser operation of our DFB laser structure and argue that the optimized core thickness prevents higher order modes from propagating in the waveguide. Fig. 4(b) shows the input–output characteristics of the optofluidic DFB laser. A clear threshold is observed at $E_{TH} = 520$ nJ. This value is nearly 20-fold lower than previous reports on evanescently pumped DFB lasers[19] and within the same order of magnitude as conventional, non-evanescently pumped liquid core waveguide lasers (90 – 157 nJ).[13] We attribute the reduction in threshold over previous evanescently pumped structures to the low index substrate material, the mixed-order grating, and the optimized core layer thickness ($d = 250$ nm). A further reduction in thickness would potentially reduce the threshold even more (compare Fig. 2(b)). However, the UV curable resist used in this work did not allow fabricating thinner layers.

Fig. 4(c) shows that the threshold pump energy for lasing depends on the dye concentration as well as the substrate

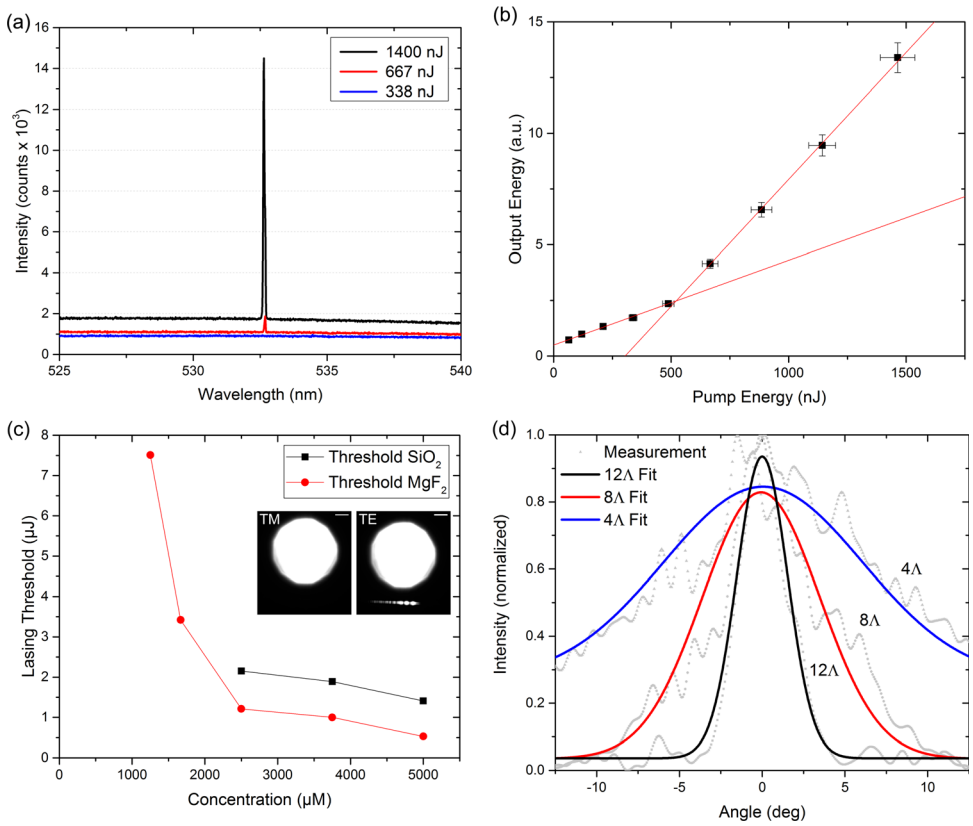

FIG. 4. (a) Emission spectra of the DFB dye laser (MgF_2 substrate; core thickness, 250 nm) using a dye concentration of 5 mM. The spectra are shown for a pump energy well below, at, and well above, the lasing threshold. Above threshold a distinct lasing peak is visible. (b) Input–output characteristics of the same DFB dye laser. The output energy increases nonlinearly with the pump energy and the lasing threshold is $E = 520$ nJ. (c) Change of the lasing threshold with dye concentration and substrate material. The inset shows a real image of the excitation area (round spot, positioned on the 1st order grating) and the region of laser emission (line-shaped area corresponding to the 2nd order area) for TE and TM polarization (scale bars, 50 μm). (d) Angular spread of the DFB laser emission depending on the number of 2nd order periods (4, 8, or 12 periods Λ, gray lines). The colored lines represent Gaussian fits to the data.

material. For high dye concentrations ($c = 2.5\,\text{mM} - 5\,\text{mM}$) the threshold energy decreases as the concentration increases, due to the higher chromophore density providing higher gain. For dye concentrations lower than 2.5 mM, there is a sudden dramatic increase in threshold energy, as cavity losses now dominate and the remaining chromophore density is not sufficient to compensate the losses.[24] In addition, the lasing threshold for MgF_2-based devices is smaller than the threshold for SiO_2-based devices which confirms the benefit of improved overlap between the laser active mode and the gain layer (see also Fig. 2(a)).

The inset in Fig. 4(c) shows a top view image of the mixed-order grating during lasing operation for TM and TE polarized emission. The circular bright area ($Ø = 250\,\mu$m) is the pump spot, which is located on the first-order grating region, and the line-shaped element is the laser emission from the second-order grating region. The laser emission is highly polarized, with lasing primarily present for TE modes. We attribute this to the higher overlap for TE modes in the waveguide with the gain region (see also Fig. 2(b)). In addition, it is clear that emission and excitation are spatially separated which is due to the design of the mixed-order grating. While optical gain and feedback occur only in the area of the pump spot, the waveguide allows modes to propagate to the second-order region where the amplified lasing mode is Bragg-scattered perpendicular to the surface.

We also analyzed the angle-resolved emission of our optofluidic DFB structures above lasing threshold. According to coupled wave theory and Eq. (2), the laser light extracted by the second-order grating should be perpendicular to the surface. However, in practice, divergence arises due to the finite size of the emission source. Figure 4(d) shows the angular spread of the emission for a series of DFB lasers with a different number of second-order periods (4, 8, and 12 periods). The emission diverges with a half width of $\Delta\theta = (3.41 \pm 0.32)^\circ$ for a DFB laser with 12 periods of second-order grating. With a decreasing number of second-order periods, the divergence of the laser emission increases, i.e., by decreasing the waist of the laser beam at the source, its angular spread increases. Hence, the divergence of a surface emitted laser beam can be tailored for different applications by adjusting the number of second-order periods to couple out the light.

In conclusion, we have presented an evanescently pumped water-based single-mode optofluidic DFB laser with a record low pump threshold of $E_{TH} = 520$ nJ. The experiment shows that the threshold of the device can be considerably decreased by choosing a low index substrate material, a mixed-order grating design, and a highly concentrated dye solution. This reduction in threshold might pave the way for applications of water based optofluidic DFB lasers in areas where evanescent pumping is required, e.g., in biosensing. Our passive and active photonic dispersion analysis enables

a precise measurement of device and grating parameters. Furthermore, the divergence of the laser emission can be tailored by the number of second-order periods used for extracting the light.

We acknowledge financial support from the European Research Council (ERC StG ABLASE, 640012), the Scottish Funding Council (via SUPA) and the European Union Marie Curie Career Integration Grant (PCIG12-GA-2012-334407). M.K. and G.L.W. acknowledge funding from the EPSRC DTG (EP/M506631/1 and EP/K503162/1). M.S. acknowledges funding from the European Commission for a Marie Sklodowska-Curie Individual Fellowship (659213). I.D.W.S. acknowledges funding from a Royal Society Wolfson research merit award. The research data supporting this publication can be accessed at http://dx.doi.org/10.17630/0ed7dad7-75e1-4ab9-9845-c455d1a7c6a4.

[1]H. Ghafouri-Shiraz, *Distributed Feedback Laser Diodes and Optical Tunable Filters* (John Wiley & Sons, 2004).
[2]I. D. W. Samuel and G. A. Turnbull, Chem. Rev. **107**, 1272 (2007).
[3]C. Vannahme, F. Maier-Flaig, U. Lemmer, and A. Kristensen, Lab Chip **13**, 2675 (2013).
[4]A. Camposeo, P. Del Carro, L. Persano, K. Cyprych, A. Szukalski, L. Sznitko, J. Mysliwiec, and D. Pisignano, ACS Nano **8**, 10893 (2014).
[5]Z. Li, Z. Zhang, T. Emery, A. Scherer, and D. Psaltis, Opt. Express **14**, 696 (2006).
[6]M. Gersborg-Hansen and A. Kristensen, Opt. Express **15**, 137 (2007).
[7]A. Bakal, C. Vannahme, A. Kristensen, and U. Levy, Appl. Phys. Lett. **107**, 211105 (2015).
[8]T. Wienhold, F. Breithaupt, C. Vannahme, M. Brøkner Christiansen, W. Dörfler, A. Kristensen, and T. Mappes, Lab Chip **12**, 3734 (2012).
[9]L. Pang, H. M. Chen, L. M. Freeman, and Y. Fainman, Lab Chip **12**, 3543 (2012).
[10]G. A. Turnbull, P. Andrew, M. J. Jory, W. L. Barnes, and I. D. W. Samuel, Phys. Rev. B **64**, 125122 (2001).
[11]P. Andrew, G. A. Turnbull, I. D. W. Samuel, and W. L. Barnes, Appl. Phys. Lett. **81**, 954 (2002).
[12]Y. Fainman, L. Lee, D. Psaltis, and C. Yang, *Optofluidics: Fundamentals, Devices, and Applications*, 1st ed. (McGraw-Hill, Inc., New York, NY, USA, 2010).
[13]W. Song, A. E. Vasdekis, Z. Li, and D. Psaltis, Appl. Phys. Lett. **94**, 051117 (2009).
[14]Z. Li, Z. Zhang, A. Scherer, and D. Psaltis, in *Proceedings of the 2008 Digest of the IEEE/LEOS Summer Topical Meetings* (2006), Vol. 14, p. 58.
[15]X. Fan and S.-H. Yun, Nat. Methods **11**, 141 (2014).
[16]M. Siddique, L. Yang, Q. Z. Wang, and R. R. Alfano, Opt. Commun. **117**, 475 (1995).
[17]M. C. Gather and S. H. Yun, Nat. Photonics **5**, 406 (2011).
[18]E. P. Ippen and C. V. Shank, Appl. Phys. Lett. **21**, 301 (1972).
[19]W. Song, A. E. Vasdekis, Z. Li, and D. Psaltis, Appl. Phys. Lett. **94**, 161110 (2009).
[20]A. B. Buckman, *Guided-Wave Photonics* (Saunders College Publishing, 1992).
[21]H. Kogelnik, J. Appl. Phys. **43**, 2327 (1972).
[22]Y. Wang, G. Tsiminis, A. L. Kanibolotsky, P. J. Skabara, I. D. W. Samuel, and G. A. Turnbull, Opt. Express **21**, 14362 (2013).
[23]C. P. Dietrich, S. Höfling, and M. C. Gather, Appl. Phys. Lett. **105**, 233702 (2014).
[24]J. Weber, Z. Phys. **258**, 277 (1973).